ADVANCED OPTICAL MATERIALS
www.advopticalmat.de

Dynamic Plasmonic Color Generation Based on Phase Transition of Vanadium Dioxide

Fang-Zhou Shu, Fang-Fang Yu, Ru-Wen Peng, Ying-Ying Zhu, Bo Xiong, Ren-Hao Fan, Zheng-Han Wang, Yongmin Liu, and Mu Wang**

Plasmonic color filtering and color printing have attracted considerable attention in recent years due to their supreme performance in display and imaging technologies. Although various color-related devices are designed, so far very few studies have touched the topic of dynamic color generation. In this article, dynamic color generation is demonstrated by integrating plasmonic nanostructures with vanadium dioxide based on its tunable optical properties through insulator–metal transition. Periodic arrays of silver nanodisks on a vanadium dioxide film are fabricated to realize different colors, relying on the excitation of localized and propagating surface plasmons, and Wood's anomaly. By tuning spatial periodicity of the arrays and diameter of the silver nanodisks, various colors can be achieved across the entire visible spectrum. Further, using insulator–metal transition of vanadium dioxide, the colors can be actively tuned by varying temperature. The approach of dynamic color generation based on the phase transition of vanadium dioxide can easily realize diverse color patterns, which makes it beneficial for display and imaging technology with distinct advantages of multifunctionality, flexibility, and high efficiency.

1. Introduction

Color filtering and color printing are essential technologies in digital displays, optical data storage, and imaging sensors. Traditionally, color generation uses pigments that absorb light at certain wavelengths to produce complementary colors. However, the spatial resolution of pigment-based color printing and display is limited to the level of 10 μm. Furthermore, it is difficult to find various pigments to reproduce all colors in the visible spectrum.[1,2] Recently, plasmonic color filtering and color printing demonstrate promising possibilities. Surface plasmons are the collective electron oscillations at a metal–dielectric interface, which include propagating surface plasmon (PSP) and localized surface plasmon (LSP), respectively.[3,4] Physically, surface plasmons enable localization and enhancement of the light field on nanoscale. Various polarization-dependent or -independent color-related devices have been designed via hole-type or pillar-type metallic nanostructures.[1,2,5–23] Plasmonic nanostructures can normally generate all the colors covering the visible spectrum by applying different structural parameters.[1,2,5–23] In addition to color filtering and color printing, plasmonics can also be harnessed for sensors,[24] photovoltaics,[25] and nanoimaging.[26]

Although plasmonic nanostructures can generate various colors on nanoscale, normally the colors cannot be reconfigurated once the structural parameters are selected. The idea of dynamic color generation is attractive since it can realize diverse color patterns, which is a feature required in practical applications.[1,2] Recently, active and tunable plasmonic devices have been proposed.[27] Tunable nanophotonic devices allow to integrate plasmonic nanostructures with graphene,[28,29] liquid crystals,[30,31] transparent conducting oxide,[32,33] and phase-transition materials.[34–36] With these materials, the amplitude, phase, and polarization of light can be easily tuned by changing external control parameters, such as the applied electric voltage or temperature. In addition, mechanically tunable optical devices have been explored as well.[37] One recent work from our group realizes a freely tunable broadband polarization rotator for terahertz waves.[38] However, despite various active optical devices have been designed, very few efforts have been devoted to dynamic color generation.[14,21,22]

Vanadium dioxide (VO_2) has been the focus of material research since its discovery.[39] The compound undergoes an insulator–metal transition around 68 °C, accompanied with structural variation from the monoclinic phase to the rutile phase. The electrical and optical properties of VO_2 undergo large changes through the phase transition, and consequently, VO_2 plays an important role in optical memory,[40] field-effect transistors,[41] modulators,[42] and intelligent windows.[43] Interestingly, the phase transition of VO_2 can also be triggered by terahertz electric field[44] and applied electrical current.[45,46] A VO_2 film can easily be fabricated by pulsed laser deposition,[42,45] the sol–gel method,[40] ratio frequency magnetron sputtering,[36,46]

F.-Z. Shu, F.-F. Yu, Prof. R.-W. Peng, Y.-Y. Zhu,
B. Xiong, Dr. R.-H. Fan, Z.-H. Wang, Prof. M. Wang
National Laboratory of Solid State Microstructures
School of Physics
Collaborative Innovation Center of Advanced Microstructures
Nanjing University
Nanjing 210093, China
E-mail: rwpeng@nju.edu.cn; muwang@nju.edu.cn
Prof. Y. Liu
Department of Mechanical and Industrial Engineering
Department of Electrical and Computer Engineering
Northeastern University
Boston, MA 02115, USA

DOI: 10.1002/adom.201700939

reactive-biased target ion beam deposition,[44] and electron beam evaporation.[47] Recently, surface plasmon resonance of silver nanoparticles on VO_2 has been successfully explored.[48–50]

In this article, we demonstrate the integration of plasmonic nanostructures and VO_2 in generating various colors dynamically for the first time. Periodic silver-nanodisk arrays are fabricated on VO_2 film in order to generate different colors, where LSP, PSP, and Wood's anomaly (WA) are excited. By designing spatial periodicity of the array and diameter of the silver nanodisks, various colors can be generated over the whole visible spectrum. Furthermore, by taking advantages of the insulator–metal transition of VO_2, we can dynamically tune the colors by changing temperature. After demonstrating physical features, we construct a pattern made of different silver-nanodisk arrays on VO_2 film to show the capability of color reconfiguration by varying the temperature.

2. Results and Discussion

2.1. Optical Properties of VO_2 Film

Before combining plasmonic nanostructures and VO_2 to generate tunable colors, we investigated the color of VO_2 films before and after the insulator–metal transition. In our study, the VO_2 films were fabricated by electron beam evaporation. The fabrication process is presented in the Experimental Section. **Figure 1**a shows the scanning electron microscope (SEM) of a VO_2 film sample. The VO_2 film is polycrystalline, featured by many nanoparticles on top. The observed major peaks in the Raman spectrum of the VO_2 film at 20 and 80 °C are consistent with literature (see Figure S1 in the Supporting Information).[45] The optical properties of VO_2 film at different temperatures were measured on a temperature stage of a UV–vis-NIR microspectrophotometer with normal and unpolarized incident light. Figure 1a also shows the reflection images of a 150 nm thick VO_2 sample at 20 and 80 °C, respectively. The size of the measured region is 100 µm. Corresponding to the temperature variation, the color of VO_2 sample changes when temperature is increased to 80 °C due to the insulator–metal transition of VO_2. It is noteworthy that the phase transition of VO_2 is reversible, and consequently the VO_2 sample can recover its original color when temperature is decreased to room temperature. Figure 1b illustrates the measured reflection spectra of the 150 nm thick VO_2 sample at 20 and 80 °C, respectively. The reflection spectrum of the VO_2 sample changes with temperature, which is due to the observed color variation. We also calculated the reflection spectra of the VO_2 sample at 20 and 80 °C, respectively, with a finite-difference time-domain software (FDTD solutions from Lumerical Inc.). The simulated reflection spectra of a 150 nm thick VO_2 sample at 20 and 80 °C are illustrated in Figure 1c. The temperature-dependent reflection spectra of the VO_2 sample are similar to that of experimental data. The small discrepancy between the experimental and simulated results can be ascribed to the difference of the VO_2 refractive index between our sample and the corresponding literature data.[51]

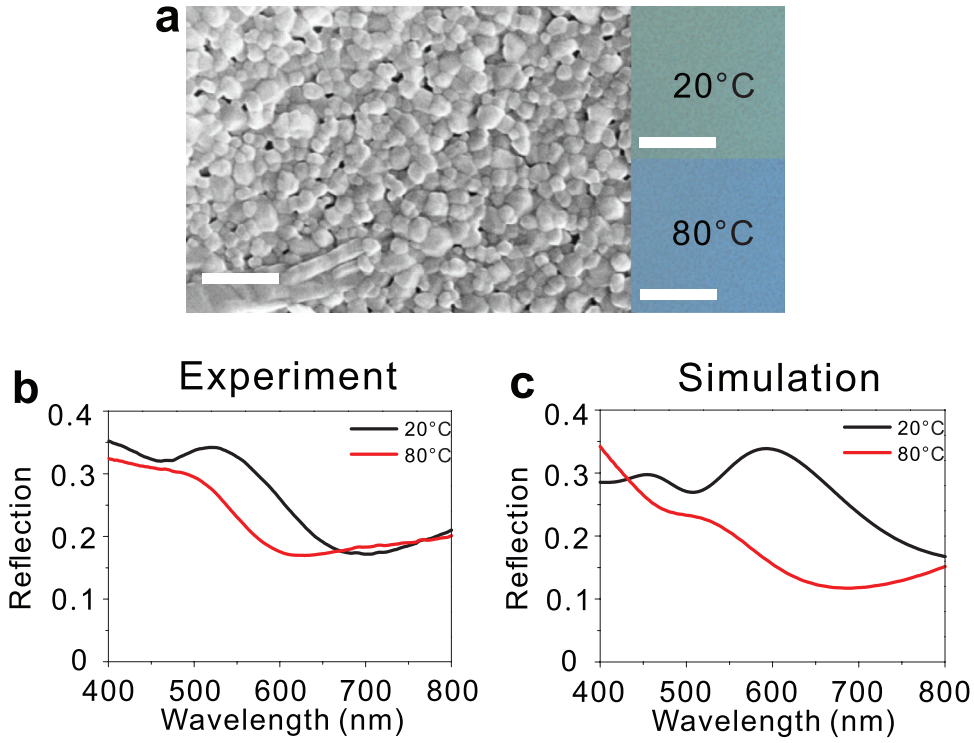

Figure 1. Optical properties of 150 nm thick VO_2 film on glass substrate. a) Scanning electron microscope (SEM) image of the VO_2 film, the scale bar represents 400 nm; reflection images of the VO_2 sample at 20 and 80 °C, the bar is 50 µm. b) Measured and c) simulated reflection spectra of the VO_2 sample at 20 and 80 °C, respectively.

2.2. Optical Properties of VO_2 Film Comprising Periodic Silver-Nanodisk Array

The tunability of color with VO_2 film alone, as that shown in Figure 1, is not sufficient to cover the entire visible spectrum. Since the resonant wavelength of plasmonic nanostructures strongly depends on their geometry and the surrounding medium, we hereby combine a VO_2 film and plasmonic nanostructures to realize active color generation. We introduce a composite structure of a VO_2 film and plasmonic nanostructures, as illustrated in **Figure 2**a. The upper layer is a 2D periodic array of silver (Ag)-nanodisks. The periods along the two orthogonal directions are identical, and the diameter of nanodisks and the spatial period of the disk array can be tailored to produce different colors. Because the imaginary component of the VO_2 refractive index in both insulating and metallic phase is nonzero for visible spectrum,[51] a silicon dioxide (SiO_2) film is used to separate the VO_2 film from the silver-nanodisk array in order to reduce the electromagnetic loss. The substrate is glass. The samples were fabricated by electron beam lithography, and experimental details are presented in the Experimental Section. Figure 2b illustrates the SEM micrograph of a sample with nanodisk diameter as 120 nm and spatial periodicity as 300 nm. Figure 2c,d shows the reflection images of the sample in Figure 2b at 20 and 80 °C, respectively. At room temperature, the sample appears greenish; however, when the temperature increases to 80 °C, the color changes to yellow due to the insulator–metal transition of VO_2. Because of the symmetry of the structure, the color of the sample is independent of the incidence polarization, which is exactly the feature required in many applications. Figure 2e shows the measured reflection spectra of the sample at 20 and 80 °C, respectively. At 20 °C, there is a peak at 560 nm in the reflection spectrum, corresponding to the greenish color. The peak shifts to 540 nm at 80 °C, and the peak width increases, resulting in the yellow color. The simulated reflection spectra of the sample at 20 and 80 °C are shown in Figure 2f. The peak wavelengths in the simulated reflection spectra at 20 and 80 °C are similar to that of the experimental results. Yet the broadening of the peak corresponding to the insulator–metal transition of VO_2 is less than that of the experimental results, which is due to the difference of VO_2 refractive index between our sample and the data in literature. Imperfection in sample fabrication may also contribute to the discrepancies of the simulated and experimental results. We also observed the reflection images and spectra of periodic silver-nanodisk array without the VO_2 film at different temperatures (see Figure S2 in the Supporting Information). It is obvious that temperature variation-induced deformations of the silver particles do not affect the colors and reflection spectra, which implies that the color changes are not related to the deformations of the silver particles.

In order to better understand the features of the reflection spectra, we analyze further the electric field distribution at the resonant wavelength. Figure 2g,h illustrates the electric field distribution at 560 nm with VO_2 in the insulating phase for *x*-polarized incidence, as calculated by FDTD simulation. One can find that the electric field mainly concentrates at the

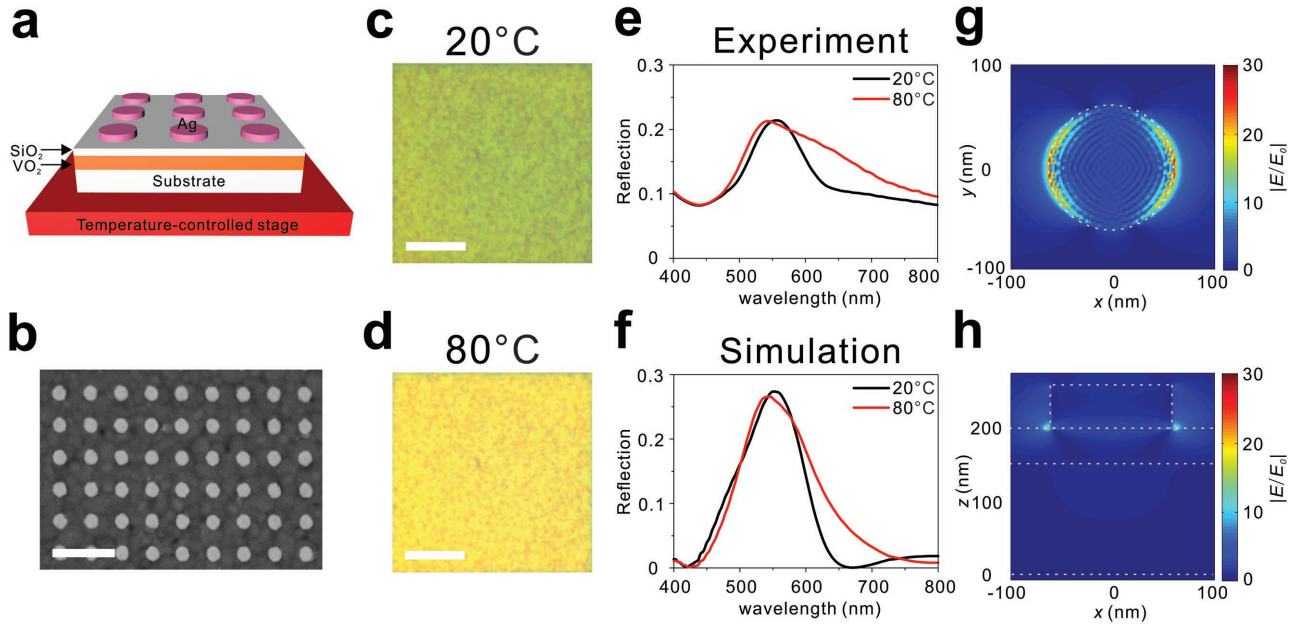

Figure 2. Optical properties of VO_2 film comprising periodic silver-nanodisk array. a) Model of the composite structure. b) SEM image of a sample with a nanodisk diameter of 120 nm and period of 300 nm; the scale bar represents 600 nm. Reflection images of the sample c) at 20 °C and d) at 80 °C, respectively; the bar length is 30 µm. e) Measured and f) simulated reflection spectra of the sample at 20 and 80 °C, respectively. g) In-plane and h) vertical cross-section electric field distribution at 560 nm with VO_2 in the insulating phase for *x*-polarized incidence, respectively, as calculated through finite-difference time-domain (FDTD) simulation.

edges of the silver nanodisk at the interface between Ag and SiO_2, which can be attributed to the LSP related to the silver nanodisk.[52] In addition, the wavelength of the LSP of a single silver nanodisk with diameter of 120 nm locates at 575 nm based on FDTD simulation, which is close to that of the resonant peak. Actually the resonant wavelength of LSP can also be determined quantitatively by solving the Clausius–Mossotti equation,[48,50,53] which satisfies

$$\lambda_{LSP} = \lambda_p \sqrt{1 + \frac{2+f}{2-2f}[1 + \sigma\varepsilon_{VO_2}(T) + (1-\sigma)\varepsilon_{SiO_2}]} \quad (1)$$

where f is the volume filling fraction of the metal nanostructure (silver nanodisk) in the composite, λ_p is the wavelength corresponding to the plasma frequency of metal (silver), and σ is the volume filling fraction of VO_2 in the VO_2–SiO_2 multilayer film, $\varepsilon_{VO_2}(T)$ is the temperature-dependent permittivity of VO_2, and ε_{SiO_2} is the permittivity of SiO_2, respectively. When VO_2 transforms from insulator to metal, the real part of the permittivity decreases while the imaginary component increases in the visible spectrum.[51] As a result, when temperature is raised to 80 °C, the peak shifts to shorter wavelengths and the peak width increases, which leads to the color transition from greenish to yellow.

2.3. Effect of Nanodisk Diameters on Optical Properties of Samples

The resonance of plasmonic nanostructures can readily be tuned by adjusting the geometric parameters of the nanodisks. **Figure 3**a shows the reflection images of samples with nanodisk diameters ranging from 100 to 190 nm with increment of 10 nm at 20 and 80 °C, respectively, whereas the spatial periodicity of the disk array remains at 300 nm. It follows that the color of the sample changes with the increase of nanodisk diameter at both 20 and 80 °C. Figure 3b–d illustrates the measured reflection spectra of samples with three selected nanodisk diameters at 20 and 80 °C (see Figure S3 in the Supporting Information for all diameters). Due to the fact that the reflection peak originates from LSP at the silver nanodisk, by increasing nanodisk diameter, the peak position shifts and broadens, leading to the generation of different colors. Yet when nanodisk diameters exceed 160 nm, even though the peak wavelength can reach 650 nm, the peak becomes too wide to generate a pure red color. In addition, the broad peak width makes color change insensitive to further increase of disk diameter, despite the fact that indeed the peak shifts to longer wavelength. Therefore, it is difficult to generate a pure red color by merely changing the nanodisk diameter. Instead, red color can be achieved by adjusting spatial

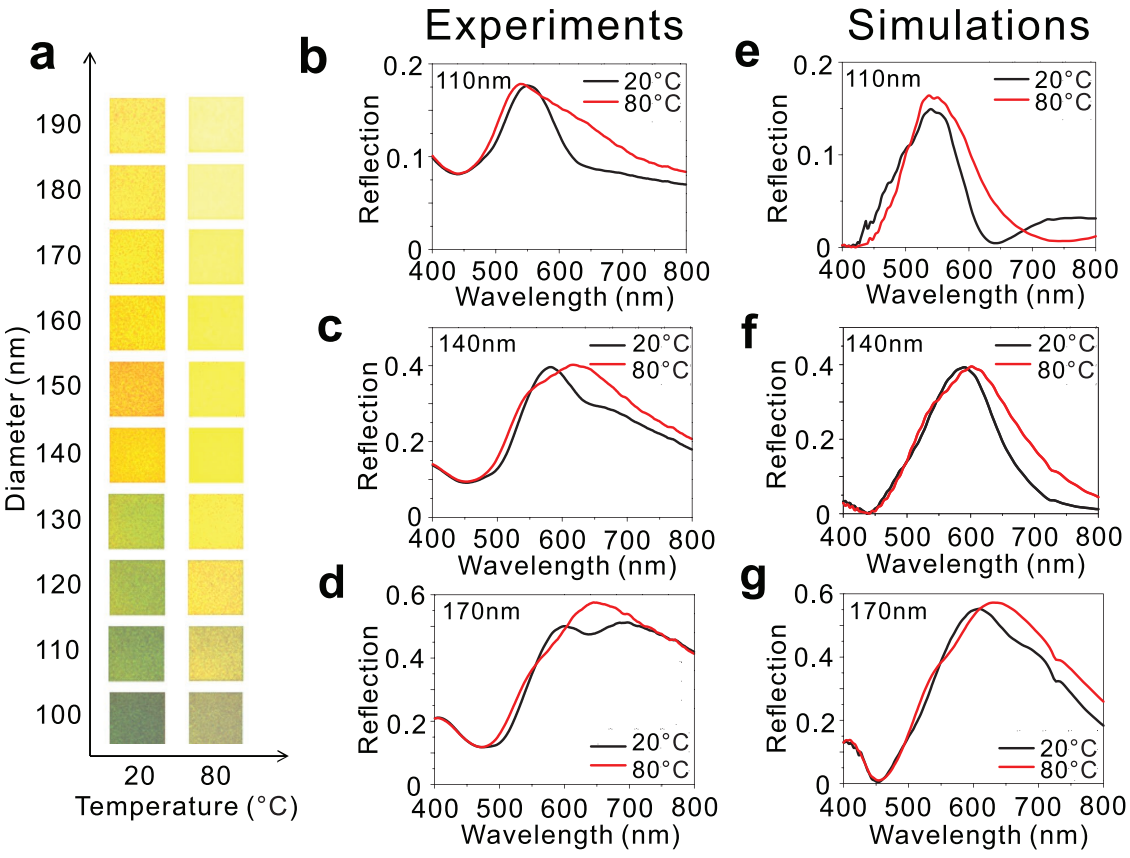

Figure 3. Optical properties of samples with different nanodisk diameters. a) Reflection images of samples with nanodisk diameters ranging from 100 to 190 nm in steps of 10 nm at 20 and 80 °C, with the period of the silver-nanodisk array fixed at 300 nm. The size of measured region is 100 µm × 100 µm. b–d) Measured reflection spectra of samples at 20 and 80 °C with nanodisk diameter of 110 nm for (b), 140 nm for (c), 170 nm for (d). e–g) Simulated reflection spectra of samples at 20 and 80 °C with nanodisk diameter of 110 nm for (e), 140 nm for (f), 170 nm for (g).

periodicity of the silver-nanodisk array. Figure 3e–g illustrates the simulated reflection spectra of samples with three selected nanodisk diameters at 20 and 80 °C (see Figure S4 in the Supporting Information for all diameters). The peak variation in the simulated reflection spectra as a function of the nanodisk diameter agrees reasonably with experimental data. In addition, we also measure the reflection images and spectra of samples with different nanodisk diameters but the thickness of SiO_2 layer decreases to 10 nm (see Figures S5 and S6 in the Supporting Information). For the same diameter of nanodisk, the color varies when the thickness of SiO_2 layer changes.

2.4. Effect of Array Period on Optical Properties of Samples

Now, we focus on the effect of spatial periodicity of the silver-nanodisk array on the reflection spectrum. A periodic metallic nanostructure can support PSP, which propagates at the interface between the metal and the dielectric, and originates from the interaction between the surface charge oscillation and the electromagnetic field of incident light.[3] The wavelength of the PSP can be expressed as[3]

$$\lambda_{\mathrm{PSP}} = \frac{P}{\sqrt{i^2 + j^2}} \sqrt{\frac{\varepsilon_{\mathrm{m}}\varepsilon_{\mathrm{d}}}{\varepsilon_{\mathrm{m}} + \varepsilon_{\mathrm{d}}}} \tag{2}$$

where P represents the spatial periodicity, ε_{m} and ε_{d} are the dielectric constants of metal and dielectric, respectively, and i and j are integers indicating the scattering orders. In addition to the PSP, the periodic metallic nanostructure can generate WA, which is related to the diffraction of light parallel to the nanostructure surface.[9,13,22,23] The wavelength of the WA can be written as[9,13]

$$\lambda_{\mathrm{WA}} = \frac{P}{\sqrt{i^2 + j^2}} \sqrt{\varepsilon_{\mathrm{d}}} \tag{3}$$

As can be inferred from these two formulas, the periodicity of the array strongly affects the wavelength of the PSP and WA. For a silver-nanodisk array with periodicity of 200, 300, and 400 nm, the wavelengths of the first-order (1,0) PSP at Ag–SiO_2 interface are 412, 505, and 630 nm, respectively, whereas the wavelengths of the first-order (1,0) WA at the Ag–SiO_2 interface occur at 292, 438, and 584 nm, respectively. The excitation of PSP and WA can affect the reflection spectrum.[1,2] Therefore, different spatial periodicities yield different reflection spectra.

Figure 4a illustrates the simulated reflection spectra of samples with different spatial periods with VO_2 in the insulating phase, with the nanodisk diameter fixed at 190 nm. When the spatial periodicity of the disk array is 300 nm, there is a wide peak at 620 nm. This peak shifts to 670 nm and the peak width decreases when the periodicity of the silver-nanodisk array increases to 400 nm. The calculated wavelength of the LSP of a single silver nanodisk with a diameter of 190 nm is 635 nm, which is very close to that of the resonant peak. In contrast, when the spatial periodicity of the disk array is selected as 300 nm, even though such structure possesses PSP and WA, the difference of the wavelength of PSP (or WA) and that of the resonant peak is large. Therefore, we conclude that the peak mainly originates from the LSP on silver nanodisk. For the silver-nanodisk array with spatial periodicity as 400 nm, however, there is a dip at 585 nm due to the occurrence of the first-order (1,0) WA. In addition, the wavelength of the first-order (1,0) PSP at Ag–SiO_2 interface approaches that of the resonant peak. Therefore, LSP tends to produce a peak in the reflection spectrum, whereas PSP and WA tend to produce a dip in the reflection spectrum.[1,2] The interaction between LSP, PSP, and WA leads to an increase in the peak wavelength and decrease in the peak width.[54] Figure 4b illustrates the electric field distribution at the peaks for a silver-nanodisk array with disk diameter as 190 nm and spatial periodicity as 300 and 400 nm, respectively. One may find that the electric field mainly focuses on the edge of the disk at the interface of Ag and SiO_2 in both cases. The electric field is more intense for the array with period of 400 nm due to the stronger interactions among LSP, PSP, and WA. Figure 4c shows the simulated reflection spectra of samples with different spatial periodicity with disk diameter as 100 nm. When the spatial periodicity decreases, the width and intensity of the peak increase, whereas the position of the peak (wavelength) remains constant. We have simulated a single silver nanodisk with disk diameter as 100 nm, which shows strong LSP resonance at 550 nm. It is very close to the resonant wavelength of the nanodisk array. For the silver-nanodisk array with spatial period as 200 nm, even though the structure can support PSP and WA, the characteristic wavelengths of PSP and WA are quite far away from 550 nm. Therefore, we conclude that the resonance peak in the simulated spectra is mainly contributed by the LSP on the silver nanodisk. For the silver-nanodisk array with periodicity of 300 nm, the wavelength of the first-order (1,0) PSP at Ag–SiO_2 interface approaches 550 nm, while the wavelength of the WA is away from that of the resonant peak. The interaction between LSP and PSP leads to a decrease in the peak width. Figure 4d shows the electric field distribution at the peaks for a silver-nanodisk array with disk diameter as 100 nm and spatial periodicity as 200 and 300 nm, respectively. Similar to that shown in Figure 4b, in both cases the electric field mainly concentrates at the edge of the silver nanodisk on the interface of Ag and SiO_2. The electric field is more intense for the array with spatial periodicity as 300 nm due to the stronger interaction between LSP and PSP.

Experiments confirm the aforementioned picture. Figure 4e shows SEM micrograph for a silver-nanodisk array with a nanodisk diameter of 190 nm and periodicity of 400 nm, and reflection images at 20 and 80 °C. The color of the sample is red at 20 °C, and it changes to orange at 80 °C due to the insulator–metal transition in VO_2. Figure 4f shows the reflection spectra of this sample. A peak appears at 660 nm in the reflection spectrum at 20 °C, which is narrower than that with nanodisk diameter as 190 nm and spatial period as 300 nm (see Figure S3j in the Supporting Information), thereby leading to the generation of red color. The peak at 660 nm splits into two peaks when temperature increases to 80 °C due to the variation in the VO_2 refractive index, therefore producing orange color. Figure 4g presents the experimental results for a silver-nanodisk array with a nanodisk diameter of 100 nm and period of 200 nm. The color of the sample is deep green at 20 °C, and it changes to blue at 80 °C. Figure 4h shows the reflection spectra of the

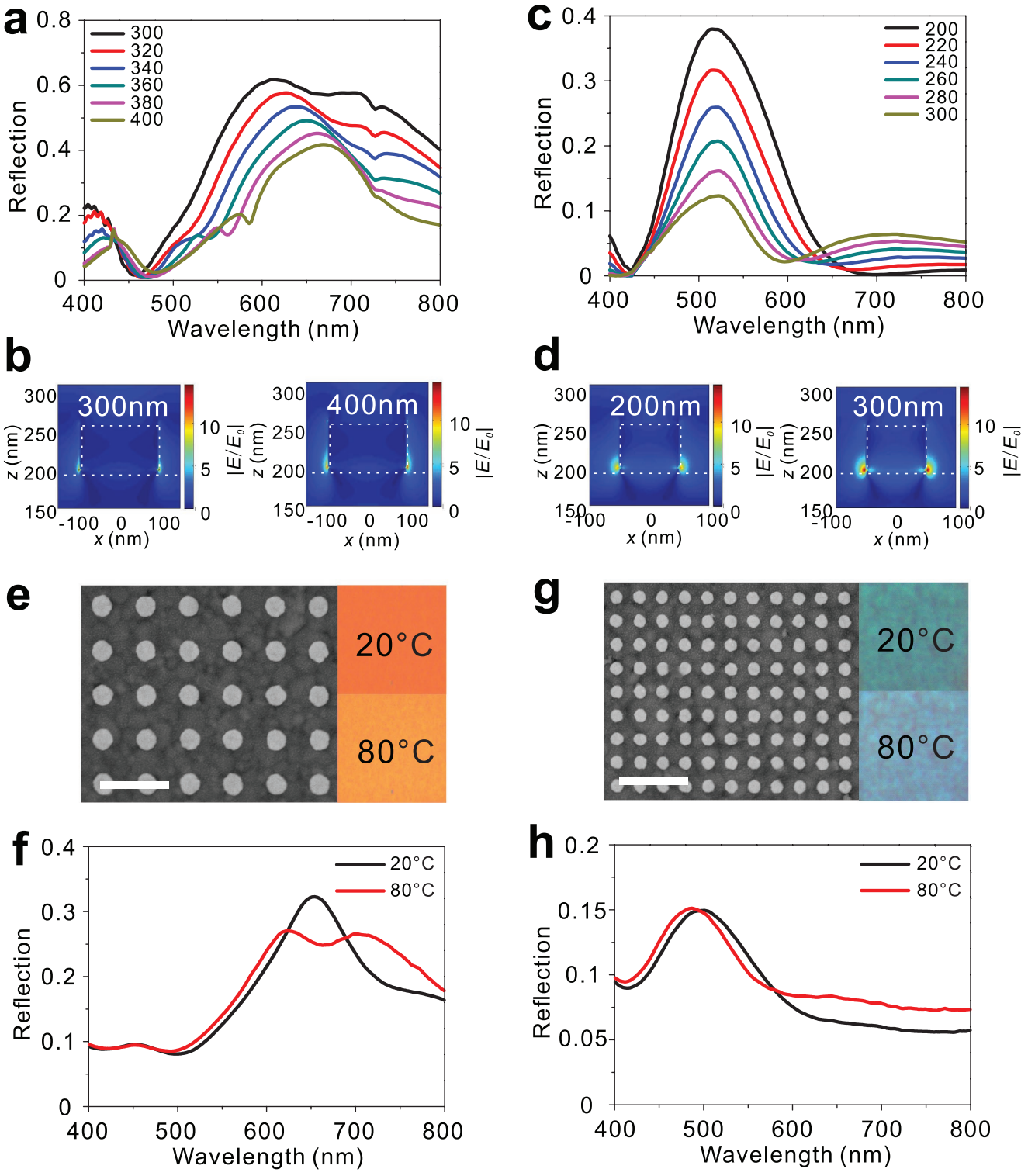

Figure 4. Effect of array period on optical properties of samples. Properties of silver-nanodisk array with a nanodisk diameter of 190 nm with VO_2 in the insulating phase: a) simulated reflection spectra of silver-nanodisk array with different periods; and b) vertical cross-section electric field distribution at peaks for silver-nanodisk array with periods of 300 and 400 nm. Properties of silver-nanodisk array with a nanodisk diameter of 100 nm with VO_2 in the insulating phase: c) simulated reflection spectra of silver-nanodisk array with different periods; and d) vertical cross-section electric field distribution at peaks for silver-nanodisk array with periods of 200 and 300 nm. e) SEM image and reflection images at 20 and 80 °C for the silver-nanodisk array with a nanodisk diameter of 190 nm and period of 400 nm. f) Reflection spectra of the sample in (e) at 20 and 80 °C. g) SEM image and reflection images at 20 and 80 °C for the silver-nanodisk array with a nanodisk diameter of 100 nm and period of 200 nm. h) Reflection spectra of the sample in (g) at 20 and 80 °C. The sizes of all reflection images are 100 μm × 100 μm, and all bars in the SEM image are 600 nm in length.

corresponding sample. We observe a peak at 500 nm in the reflection spectrum at 20 °C corresponding to deep green. The peak in the reflection spectra shifts to 480 nm when temperature increases to 80 °C, and the sample appears as blue.

2.5. Color Reconfiguration of a Pattern

Thus far, we have demonstrated a temperature-dependent color change on a VO_2 film comprising a periodic silver-nanodisk array. When the temperature changes, the colors of samples vary because of the insulator–metal transition of VO_2. To quantify this effect, we calculate the chromaticity coordinates based on the measured reflection spectra of the various sample structures at 20 and 80 °C presented in Figures S3 and S6 (Supporting Information) and Figure 4, and plot the coordinates in the International Commission on Illumination (CIE) 1931 chromaticity diagram, as shown in **Figure 5**a,b, respectively. The chromaticity coordinates change when the nanodisk diameter, the spatial periodicity, and the applied temperature are changed. These colors in the chromaticity diagram are close to that observed by a charge-coupled device detector.

Since we can realize abundant colors by using VO_2 and periodic silver-nanodisk arrays, we can construct a temperature-dependent color image on VO_2 film. **Figure 6**a,b demonstrates the SEM micrograph of a pattern containing five different structures. As shown in Figure 6b, four regions of the sample comprise periodic silver-nanodisk arrays with different nanodisk diameters and periods, while the rest of the area does not possess any array. The reflection images of the pattern at 20 and 80 °C are shown in Figure 6c,d. One may find that five colors can be identified in the image at 20 °C depending on different microstructures shown in Figure 6a,b. When temperature increases to 80 °C, the colors of the image change simultaneously due to the insulator–metal transition of VO_2. Thereafter, when the sample is cooled down to room temperature, the sample resumes to its original colors due to the reversibility of the phase transition of VO_2. Actually, the colors of the image can vary with further decreasing the thickness of SiO_2 layer. As shown in Figure 6e, the pattern has the same nanostructure in Figure 6a, but the thickness of SiO_2 layer is decreased to 10 nm. We can find that once the temperature increases to 80 °C, the colors of the image also change, as illustrated in Figure 6f. It is indicated that some of the color changes come from the fact that the VO_2 film changes its color when its insulator–metal transition happens, while some of the color changes may originate mainly from the different behavior of LSP in the systems before or after insulator–metal transition of VO_2, and they are also slight influenced by small variation of both PSP and WA due to insulator–metal transition of VO_2. In this way, we are able to make any pattern with multiple colors on the VO_2 film by designing different nanostructures, and we can reconfigure colors by changing temperature. In principle, the spatial resolution of this approach can be less than the unit size of the nanostructure.

3. Conclusion

In conclusion, we realize abundant color variation on a VO_2 film comprising periodic arrays of silver nanodisks, where the color can dynamically be tuned via the insulator–metal transition of VO_2. Since the surface plasmon resonance is sensitive to the geometrical parameters of the silver nanodisk array, we can design different plasmonic nanostructures to display rich color variation beyond the diffraction limit.[5] Recently, the aluminum-based

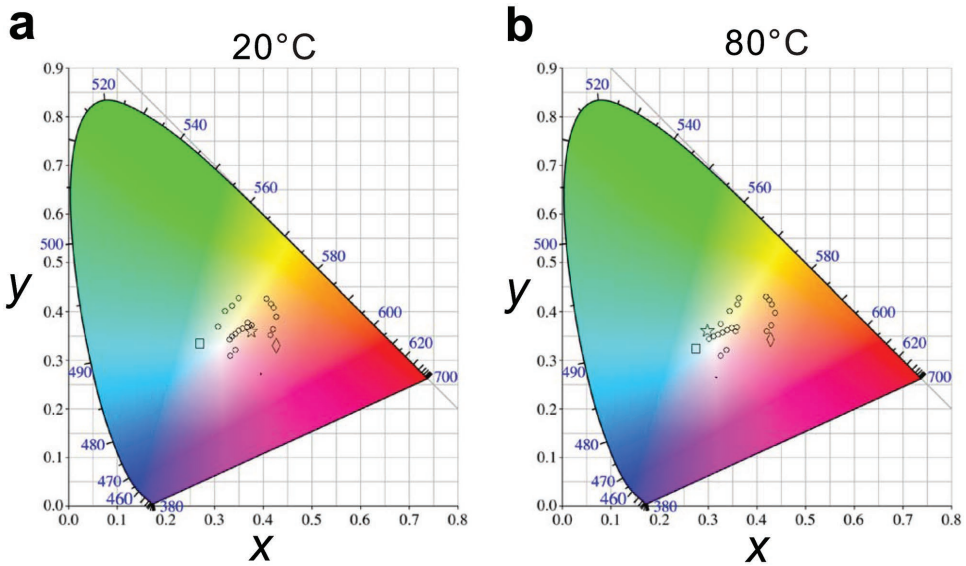

Figure 5. Color range of the composite structure in the CIE 1931 chromaticity diagram. Chromaticity coordinates corresponding to the measured reflection spectra in Figures S3 and S6 (Supporting Information) and Figure 4 for a) at 20 °C and b) at 80 °C, respectively. The 20 circular points correspond to silver-nanodisk arrays with a period of 300 nm and nanodisk diameters ranging from 100 to 190 nm in steps of 10 nm, with the thickness of SiO_2 layer of 50 and 10 nm. The diamond symbol corresponds to the silver-nanodisk array with a nanodisk diameter of 190 nm and period of 400 nm. The rectangular symbol corresponds to the silver-nanodisk array with a nanodisk diameter of 100 nm and period of 200 nm. The star symbol corresponds to the region without a silver-nanodisk array.

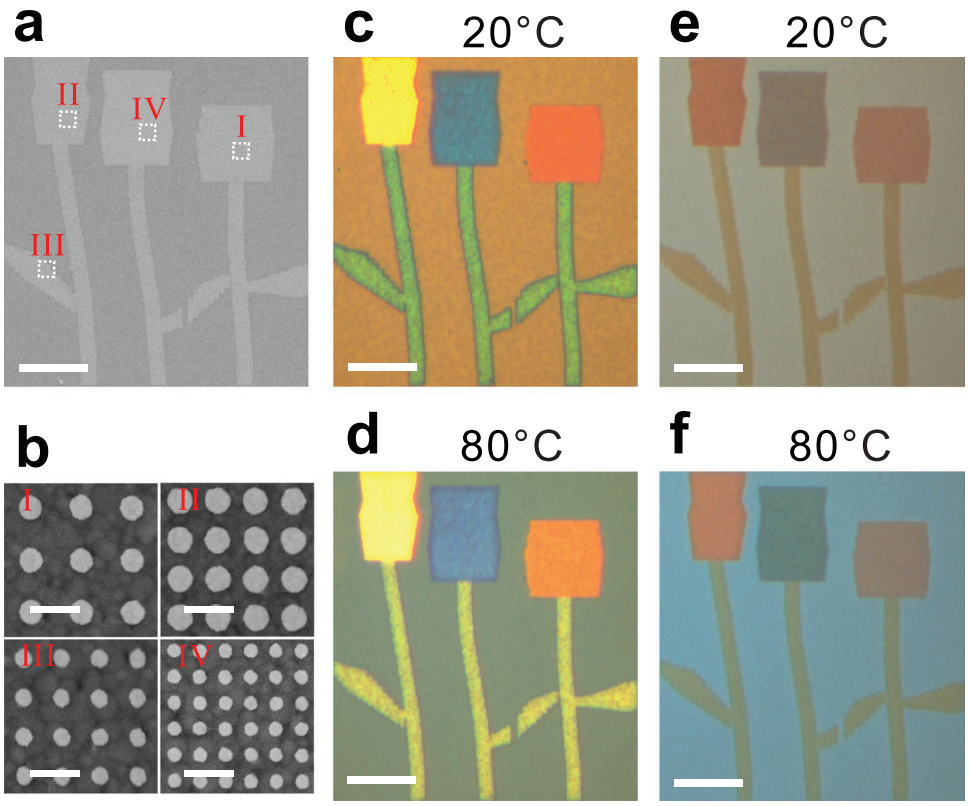

Figure 6. Optical properties of a pattern containing five different structures. a) SEM image of the pattern; the bar is 40 µm in length. b) Magnified SEM images of the four array-containing regions, where all bars are 400 nm in length. Reflection images of the pattern c) at 20 °C and d) at 80 °C, respectively; the bar is 40 µm in length. Reflection images of a pattern e) at 20 °C and f) at 80 °C, respectively, where the pattern has the same nanostructure as the nanostructure in (a) but the thickness of SiO_2 layer is decreased to 10 nm; the bar is 40 µm in length.

plasmonics approach has become popular in designing various colors because of its advantage of low cost, good stability, and compatibility with the complementary metal-oxide-semiconductor technology.[6,7,10,12–15,17–19,21] We expect that it is possible to replace silver with aluminum in our design. In addition to the nanodisks, other polarization-dependent structures can also be applied to design various colors for special applications. Although the colors of the VO_2 composite structures change with longer response time, which is a typical diffusion-related feature, it may change much faster by introducing electrical current.[45,46] Instead of using VO_2, we may use other optically tunable materials to integrate plasmonic nanostructures to dynamically control color.[27–35] We should also point out that although we have focused on the dynamic color generation in the reflection mode, it is also possible to realize color variation in transmission mode based on similar mechanism. Our study opens a paradigm for display and imaging with distinct advantages of multifunctionality, flexibility, and high efficiency.

4. Experimental Section

Sample Fabrication: A 75 nm thick vanadium (V) layer was first deposited on a glass substrate via electron beam evaporation with a rate of 0.5 Å s^{-1} and a base pressure of 1×10^{-5} Torr. The V film was transformed into a VO_2 film with a thickness of 150 nm after heat annealing for 180 min in oxygen at 450 °C under a pressure of 10 Pa. Then, a 50 nm thick SiO_2 layer was deposited on the VO_2 film by electron beam evaporation at a rate of 1 Å s^{-1} and a base pressure of 1×10^{-5} Torr. Subsequently, a 120 nm thick positive electron beam resist (AR-P 672.03) was spin coated onto the sample. The sample was then exposed via electron beam lithography with acceleration voltage of 30 kV, working distance of 9.5 mm, and area dose of 450 µC cm^{-2}. The write-field size was 200 µm × 200 µm with a step size of 10 nm. After exposure, the resist was developed in a developer (X AR 600–56) for 90 s and subsequently rinsed in isopropyl alcohol for 30 s. Next, a 60 nm thick silver layer was deposited on the sample using electron beam evaporation with rate of 1 Å s^{-1} and base pressure of 1×10^{-5} Torr. Finally, lift-off was carried out in a remover (AR 300–76) at 80 °C after 1 h.

SEM and Optical Characterization: The sample morphology was observed by a field-emission scanning electron microscope (Zeiss, ULTRA 55). The Raman spectrum of the VO_2 film at 20 and 80 °C was obtained by a confocal micro-Raman system (Princeton Instruments). The laser wavelength was 514.5 nm, and the spot size was about 2 µm. For optical measurements, the samples were placed on a temperature-stage, and the reflection spectra of the samples at different temperatures were measured by a UV-visible-NIR microspectrophotometer (CRAIC QDI2010) in normal and unpolarized incidence with a halogen source. The reflection color images of the samples at different temperatures were captured by a charge-coupled device equipped with a UV–vis-NIR microspectrophotometer.

Numerical Simulation: The simulated reflection spectra of the samples were calculated by FDTD software (FDTD solutions from Lumerical Inc.). In the simulation, periodic boundary conditions were applied in both the *x*- and *y*-directions, and perfectly matched layers were applied in the *z*-direction. The *x*-polarized plane wave for normal

incidence was considered. The VO_2 refractive index in the metallic and insulating phases was taken from literature,[51] and the refractive-index data for SiO_2 and Ag were from literature as well.[55]

Supporting Information

Supporting Information is available from the Wiley Online Library or from the author.

Acknowledgements

This work was supported by the National Key R&D Program of China (2017YFA0303702), the National Natural Science Foundation of China (Grant Nos. 11634005, 61475070, 11474157, 11674155, 11621091, and 11604143), the Ministry of Science and Technology of China (Grant No. 2014CB921103), and partially by the "333 project" from the Jiangsu province (BRA2016350). And, Y.L. was partially supported by the Office of Naval Research under Grant number N00014-16-1-2409.

Conflict of Interest

The authors declare no conflict of interest.

Keywords

dynamic color generation, insulator–metal transition, plasmonic nanostructures, vanadium dioxide

Received: September 1, 2017
Revised: January 8, 2018
Published online:

[1] Y. Gu, L. Zhang, J. K. W. Yang, S. P. Yeo, C.-W. Qiu, *Nanoscale* **2015**, *7*, 6409.
[2] A. Kristensen, J. K. W. Yang, S. I. Bozhevolnyi, S. Link, P. Nordlander, N. J. Halas, N. A. Mortensen, *Nat. Rev. Mater.* **2016**, *2*, 16088.
[3] W. L. Barnes, A. Dereux, T. W. Ebbesen, *Nature* **2003**, *424*, 824.
[4] J. A. Schuller, E. S. Barnard, W. Cai, Y. C. Jun, J. S. White, M. L. Brongersma, *Nat. Mater.* **2010**, *9*, 193.
[5] K. Kumar, H. Duan, R. S. Hedge, S. C. W. Koh, J. N. Wei, J. K. W. Yang, *Nat. Nanotechnol.* **2012**, *7*, 557.
[6] T. Ellenbogen, K. Seo, K. B. Crozier, *Nano Lett.* **2012**, *12*, 1026.
[7] S. Yokogawa, S. P. Burgos, H. A. Atwater, *Nano Lett.* **2012**, *12*, 4349.
[8] G. Si, Y. Zhao, J. Lv, M. Lu, F. Wang, H. Liu, N. Xiang, T. J. Huang, A. J. Danner, J. Teng, Y. J. Liu, *Nanoscale* **2013**, *5*, 6243.
[9] M. R. Gartia, A. Hsiao, A. Pokhriyal, S. Seo, G. Kulsharova, B. T. Cunningham, T. C. Bond, G. L. Liu, *Adv. Opt. Mater.* **2013**, *1*, 68.
[10] B. Y. Zheng, Y. Wang, P. Nordlander, N. J. Halas, *Adv. Mater.* **2014**, *26*, 6318.
[11] A. S. Roberts, A. Pors, O. Albrektsen, S. I. Bozhevolnyi, *Nano Lett.* **2014**, *14*, 783.
[12] J. S. Clausen, E. Højlund-Nielsen, A. B. Christiansen, S. Yazdi, M. Grajower, H. Taha, U. Levy, A. Kristensen, N. A. Mortensen, *Nano Lett.* **2014**, *14*, 4499.
[13] V. R. Shrestha, S.-S. Lee, E.-S. Kim, D.-Y. Choi, *Nano Lett.* **2014**, *14*, 6672.
[14] D. Franklin, Y. Chen, A. Vazquez-Guardado, S. Modak, J. Boroumand, D. Xu, S.-T. Wu, D. Chanda, *Nat. Commun.* **2015**, *6*, 7337.
[15] J. Xue, Z.-K. Zhou, Z. Wei, R. Su, J. Lai, J. Li, C. Li, T. Zhang, X.-H. Wang, *Nat. Commun.* **2015**, *6*, 8906.
[16] E. Segal, A. Weissman, D. Gachet, A. Salomon, *Nanoscale* **2016**, *8*, 15296.
[17] Z. Li, A. W. Clark, J. M. Cooper, *ACS Nano* **2016**, *10*, 492.
[18] J. Olson, A. Manjavacas, T. Basu, D. Huang, A. E. Schlather, B. Zheng, N. J. Halas, P. Nordlander, S. Link, *ACS Nano* **2016**, *10*, 1108.
[19] M. Miyata, H. Hatada, J. Takahara, *Nano Lett.* **2016**, *16*, 3166.
[20] K. Xiong, G. Emilsson, A. Maziz, X. Yang, L. Shao, E. W. H. Jager, A. B. Dahlin, *Adv. Mater.* **2016**, *28*, 9956.
[21] T. Xu, E. C. Walter, A. Agrawal, C. Bohn, J. Velmurugan, W. Zhu, H. J. Lezec, A. A. Talin, *Nat. Commun.* **2016**, *7*, 10479.
[22] X. Duan, S. Kamin, N. Liu, *Nat. Commun.* **2017**, *8*, 14606.
[23] H. Wang, X. Wang, C. Yan, H. Zhao, J. Zhang, C. Santschi, O. J. F. Martin, *ACS Nano* **2017**, *11*, 4419.
[24] J. N. Anker, W. P. Hall, O. Lyandres, N. C. Shah, J. Zhao, R. P. Van Duyne, *Nat. Mater.* **2008**, *7*, 442.
[25] H. A. Atwater, A. Polman, *Nat. Mater.* **2010**, *9*, 205.
[26] S. Kawata, Y. Inouye, P. Verma, *Nat. Photonics* **2009**, *3*, 388.
[27] N. I. Zheludev, Y. S. Kivshar, *Nat. Mater.* **2012**, *11*, 917.
[28] Y. Yao, M. A. Kats, P. Genevet, N. Yu, Y. Song, J. Kong, F. Capasso, *Nano Lett.* **2013**, *13*, 1257.
[29] Y. Zhou, C. Wang, D. H. Xu, R. H. Fan, K. Zhang, R. W. Peng, Q. Hu, M. Wang, *Europhys. Lett.* **2014**, *107*, 34007.
[30] X. Wang, D.-H. Kwon, D. H. Werner, I.-C. Khoo, A. V. Kildishev, V. M. Shalaev, *Appl. Phys. Lett.* **2007**, *91*, 143122.
[31] A. E. Cetin, A. Mertiri, M. Huang, S. Erramilli, H. Altug, *Adv. Opt. Mater.* **2013**, *1*, 915.
[32] Y.-W. Huang, H. W. H. Lee, R. Sokhoyan, R. A. Pala, K. Thyagarajan, S. Han, D. P. Tsai, H. A. Atwater, *Nano Lett.* **2016**, *16*, 5319.
[33] J. Park, J.-H. Kang, S. J. Kim, X. Liu, M. L. Brongersma, *Nano Lett.* **2017**, *17*, 407.
[34] X. Yin, M. Schäferling, A.-K. U. Michel, A. Tittl, M. Wuttig, T. Taubner, H. Giessen, *Nano Lett.* **2015**, *15*, 4255.
[35] Q. Wang, E. T. F. Rogers, B. Gholipour, C.-M. Wang, G. Yuan, J. Teng, N. I. Zheludev, *Nat. Photonics* **2015**, *10*, 60.
[36] J. Rensberg, S. Zhang, Y. Zhou, A. S. McLeod, C. Schwarz, M. Goldflam, M. Liu, J. Kerbusch, R. Nawrodt, S. Ramanathan, D. N. Basov, F. Capasso, C. Ronning, M. A. Kats, *Nano Lett.* **2016**, *16*, 1050.
[37] N. I. Zheludev, E. Plum, *Nat. Nanotechnol.* **2016**, *11*, 16.
[38] R. H. Fan, Y. Zhou, X. P. Ren, R. W. Peng, S. C. Jiang, D. H. Xu, X. Xiong, X. R. Huang, M. Wang, *Adv. Mater.* **2015**, *27*, 1201.
[39] Z. Yang, C. Ko, S. Ramanathan, *Annu. Rev. Mater. Res.* **2011**, *41*, 337.
[40] T. Driscoll, H.-T. Kim, B.-G. Chae, B.-J. Kim, Y.-W. Lee, N. M. Jokerst, S. Palit, D. R. Smith, M. Di Ventra, D. N. Basov, *Science* **2009**, *325*, 1518.
[41] S. Hormoz, S. Ramanathan, *Solid-State Electron.* **2010**, *54*, 654.
[42] K. Appavoo, R. F. Haglund, *Sci. Rep.* **2014**, *4*, 6771.
[43] S.-Y. Li, G. A. Niklasson, C. G. Granqvist, *Thin Solid Films* **2012**, *520*, 3823.
[44] M. Liu, H. Y. Hwang, H. Tao, A. C. Strikwerda, K. Fan, G. R. Keiser, A. J. Sternbach, K. G. West, S. Kittiwatanakul, J. Lu, S. A. Wolf, F. G. Omenetto, X. Zhang, K. A. Nelson, R. D. Averitt, *Nature* **2012**, *487*, 345.
[45] H.-T. Kim, B.-G. Chae, D.-H. Youn, G. Kim, K.-Y. Kang, S.-J. Lee, K. Kim, Y.-S. Lim, *Appl. Phys. Lett.* **2005**, *86*, 242101.
[46] L. Liu, L. Kang, T. S. Mayer, D. H. Werner, *Nat. Commun.* **2016**, *7*, 13236.

[47] R. E. Marvel, K. Appavoo, B. K. Choi, J. Nag, R. F. Haglund, *Appl. Phys. A: Mater. Sci. Process.* **2013**, *111*, 975.
[48] G. Xu, Y. Chen, M. Tazawa, P. Jin, *J. Phys. Chem. B* **2006**, *110*, 2051.
[49] P. Jin, M. Tazawa, G. Xu, *J. Appl. Phys.* **2006**, *99*, 096106.
[50] G. Xu, C.-M. Huang, P. Jin, M. Tazawa, D.-M. Chen, *J. Appl. Phys.* **2008**, *104*, 053101.
[51] H. W. Verleur, A. S. Barker, C. N. Berglund, *Phys. Rev.* **1968**, *172*, 788.
[52] S. A. Maier, *Plasmonics: Fundamentals and Applications*, Springer, New York **2007**.
[53] W. Cai, V. Shalaev, *Optical Metamaterials: Fundamentals and Applications*, Springer, New York **2010**.
[54] Y. J. Bao, R. W. Peng, D. J. Shu, M. Wang, X. Lu, J. Shao, W. Lu, N. B. Ming, *Phys. Rev. Lett.* **2008**, *101*, 087401.
[55] E. D. Palik, *Handbook of Optical Constants of Solids*, Academic Press, San Diego, CA, USA **1985**.